International Journal of Minerals, Metallurgy and Materials
Volume 21, Number 8, August 2014, Page 755
DOI: 10.1007/s12613-014-0968-8

Influence of silicon on the microstructures, mechanical properties and stretch-flangeability of dual phase steels

Le-yu Zhou, Dan Zhang, and Ya-zheng Liu

School of Materials Science and Engineering, University of Science and Technology Beijing, Beijing 100083, China
(Received: 21 November 2013; revised: 14 March 2014; accepted: 20 March 2014)

Abstract: Uniaxial tension tests and hole-expansion tests were carried out to determine the influence of silicon on the microstructures, mechanical properties, and stretch-flangeability of conventional dual-phase steels. Compared to 0.03wt% silicon, the addition of 1.08wt% silicon induced the formation of finer ferrite grains (6.8 μm) and a higher carbon content of martensite ($C_m \approx 0.32$wt%). As the silicon level increased, the initial strain-hardening rate (n value) and the uniform elongation increased, whereas the yield strength, yield ratio, and stretch-flangeability decreased. The microstructures were observed after hole-expansion tests. The results showed that low carbon content martensite ($C_m \approx 0.19$wt%) can easily deform in coordination with ferrite. The relationship between the mechanical properties and stretch-flangeability indicated that the steel with large post-uniform elongation has good stretch-flangeability due to a closer plastic incompatibility of the ferrite and martensite phases, which can effectively delay the production and decohesion of microvoids.

Keywords: dual-phase steel; silicon content; mechanical properties; microstructure; strain hardening

1. Introduction

Dual-phase (DP) steels that contain a soft ferrite phase matrix and a hard second-phase martensite combine high strength with good formability and weldability. They are widely used in the automotive industry as structural members and security components. In the last few decades, the microstructures, chemical composition, mechanical properties, and formability of these kinds of steels have been extensively studied [1−10].

The stretch-flangeability of these strip steels is usually described by the hole-expansion ratio (HER, represented by λ), which is affected by microstructures [3]. The formability of transformation induced plasticity steel (TRIP) has been studied by Sugimoto *et al.* [11] and Nagasaka *et al.* [12]. Hyun *et al*. [8] have studied the estimation of hole flangeability for ferrite-bainite (F + B) duplex steels and TRIP steels. F + B steel has a better hole flangeability than TRIP steel if estimated by minimum hole diameter, while TRIP steel has a better formability than F + B steel from the viewpoint of lip shape accuracy and lip height. A qualitative analysis was carried out on the formability of DP steels by introducing a realistic microstructure-based finite element approach by Kim *et al.* [9]. It was inferred that the localized plastic deformation in the ferritic phase might be closely related to the macroscopic formability of DP steels.

The mechanical properties and HER of steel are closely related because the mechanical properties of steel affect its stretch-flangeability. During hole expansion, deformation in the circumferential direction at the edge of the center hole is stretching while in the longitudinal direction it is bending. Although the hole-expansion test is obviously different from the uniaxial tension test, the contraction strain after being hole-expanded is only in the thickness direction, while in the uniaxial tension test, the contraction strains are both in the width and thickness directions. After analyzing the stresses and strains during hole-expansion tests, Yamada and Koide [13] confirmed that the stress state in the vicinity of the center hole is uniaxial tension. Studies on local plastic strain and microvoid formation in necked regions during the tensile test therefore provide a basis with respect to the

Corresponding author: Ya-zheng Liu E-mail: lyzh@ustb.edu.cn
© University of Science and Technology Beijing and Springer-Verlag Berlin Heidelberg 2014

hole-expansion test. Ghadbeigi *et al.* [14] have studied the local strain distributions within the ferrite–martensite (F–M) microstructure using digital image correlation (DIC) and *in-situ* tensile testing inside a scanning electron microscope throughout a tensile test. The results show that, in some areas, both the martensite and ferrite phases experience large plastic deformation during the tensile test, with local strain values up to 110% and 130%, respectively, for an applied strain of 42%. This shows that some martensites have good plastic deformation ability. The localized bands of deformation are located either inside large ferrite grains or very close to the interface between ferrite and martensite, with small ferrite grains trapped between several islands of martensite. In tensile tests of DP steel, Steinbrunner *et al.* [7] observed three apparent void nucleation mechanisms: decohesion at the F–M interface, separation of fractured martensite particles, and separation of adjacent or deformed martensite particles. To examine the different local strain distributions in different places where microvoids form, the carbon content and martensite morphology [15–19] should be taken into consideration.

HER is also affected by micro-alloying elements [3,20], the quality of sheared edges [9–10], hole diameter, and strip thickness [8].

The observation of microstructure evolution in DP steels during hole-expansion tests is rarely done. This study aimed at a detailed description of the relationship between Si content and the microstructures, mechanical properties, and stretch-flangeability of dual-phase steels. The microstructures and mechanical properties of steels with 1.08wt% and 0.03wt% Si, the microstructure evolution during hole-expansion tests, and the relationship between the strain-hardening behavior and stretch-flangeability were investigated.

2. Experimental

Two commercial DP steels were used in this study. Both steels contained 0.07wt% C, 1.2wt% Mn, 0.47wt% Cr, 0.013wt% P, and 0.004wt% S, but they differed in Si content, 1.08wt% vs. 0.03wt%. These were named high Si (HSi) and low Si (LSi) steels, respectively.

The steels were rolled in a 2250 mm hot-rolling mill line. The processing schedule is outlined in Fig. 1. To obtain the final ferrite/martensite dual-phase microstructure, the steels were subjected to online multiple-step cooling. The final thickness of the strips was 4 mm.

Tensile test specimens were machined with a gage length of 50 mm. The applied tensile loading axis corresponded to the rolling direction of the strips. Tensile tests were performed at room temperature with a constant cross-head displacement rate of 0.5 mm/min on a CMT4105 100 kN testing machine. Due to the continuous character of DP steels, the yield strength is given as the 0.2% offset yield strength. The uniform elongation was determined as the strain at which the true strain (ε_t) equals the strain-hardening rate ($d\sigma_t/d\varepsilon_t$). The strain-hardening behavior of HSi and LSi steels was analyzed using Hollomon, differential Crussard–Jaoul (D_{C-J}), and modified Crussard–Jaoul (M_{C-J}) analyses.

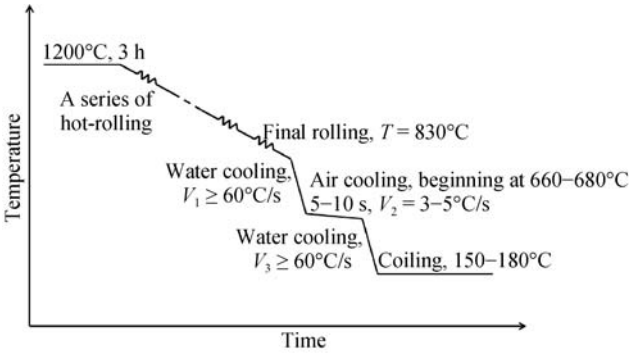

Fig. 1. Thermomechanical processing routes to produce DP steels in a thermomechanically controlled process (TMCP).

In the present study, hole-expansion tests were conducted on a BCS-50A strip-forming testing machine. To avoid crack formation at small strain in the punching method, 10 mm diameter holes were wire-cut at the center of 100 mm × 100 mm square specimens. In this way, the surface quality was modified and HER was improved, making it more suitable for studying the stretch-flangeability. Holes were expanded with a conical punch having an angle of 60° as shown in Fig. 2. The holder force was 20 kN and the punch speed was 20 mm/min. The punch advance was stopped at the occurrence of a crack through the thickness. The λ-value was defined by the following equation:

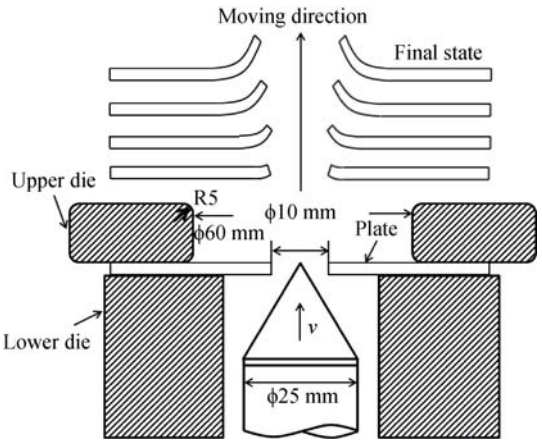

Fig. 2. Schematic diagram of hole-expanding test.

$$\lambda = \frac{d_1 - d_0}{d_0} \times 100\% \quad (1)$$

where d_0 is the diameter of the hole before expansion and d_1 is the diameter of the hole when a crack is observed through the thickness.

Samples for scanning electron microscopy (SEM) were mechanically ground and polished. In addition, the samples were deeply etched in a 4% nital solution to reveal the microstructure. The mean ferrite grain size (d_f) and the martensite volume fraction (f_m) were determined on metallographs using Image Tool software. A TECNAI F-20 transmission electron microscope (TEM) was used to observe the deformation of the dislocation structures.

3. Results and discussion

3.1. Microstructures

SEM micrographs of HSi and LSi steels (Fig. 3) show that the microstructures (morphology, size, ferrite and martensite distribution) are quite different for the two steels. The d_f values are 6.8 and 8.9 μm, and the f_m values are around 25% and 32%, for the HSi and LSi steels, respectively (Table 1).

According to the mass balance calculation, the carbon content of martensite (C_m) can be determined from the following equation:

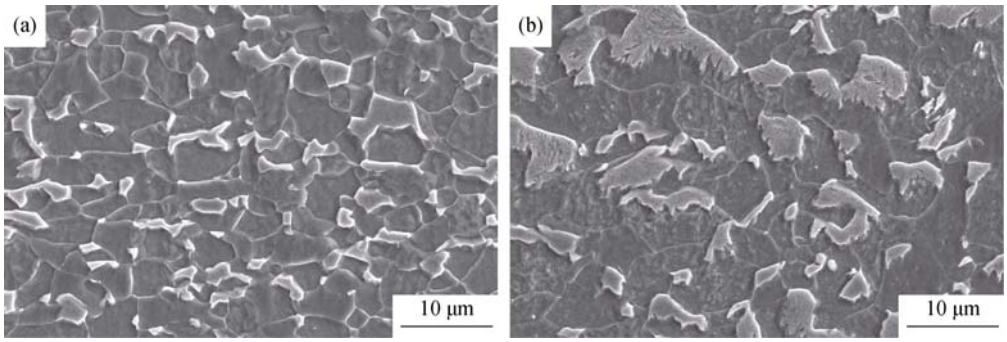

Fig. 3. SEM images showing the original microstructures of test steels: (a) HSi steel and (b) LSi steel.

Table 1. Comparison of microstructure parameters obtained from SEM micrographs and tensile data between HSi (1.08wt%) and LSi (0.03wt%) DP steels

Steel	d_f/ μm	f_m / %	C_m / wt%	YS / MPa	UTS / MPa	UE / %	TE / %	Yield ratio	λ / %
HSi	6.8	25	0.32	380	730	18.2	25.1	0.52	76
LSi	8.9	32	0.19	462	655	14.3	26.2	0.71	130

Note: d_f—ferrite grain size, f_m—martensite volume fraction, C_m—carbon content of martensite, YS—yield strength, UTS—ultimate tensile strength, UE—uniform elongation, TE—total elongation, and λ—hole-expansion ratio.

$$C_m = \frac{C_C - (1 - f_m)C_f}{f_m} \quad (2)$$

where C_C is the carbon content of the composite, C_f is the carbon content of ferrite, and f_m is the martensite volume fraction. The carbon content of ferrite was assumed to be 0.015 [21], which is the soluble carbon content in ferrite at room temperature. C_m obtained from Eq. (2) is given in Table 1.

For the HSi steel, fine and equiaxial ferrite grains were obtained, as shown in Fig. 3(a). The martensite islands were small and dispersively distributed, with most of them having angular geometry and well-defined F–M phase boundaries. Previous work [22–23] indicated that the formation of fine and equiaxial ferrite in response to Si addition is the result of an increased nucleation rate of ferrite. This is attributed to the fact that Si increases the activity of carbon in austenite by inhibiting carbide formation, thereby increasing the driving force for the γ → α transformation. Consequently, residual austenite is severely segmented by proeutectoid ferrite and leads to the formation of dispersed martensite. For the LSi steel, large ferrite grains and bulky martensite islands were obtained, as shown in Fig. 3(b). Some of the F–M phase boundaries were not smooth and the interior of the martensite was veined.

It has been reported that Si promotes carbon enrichment in metastable austenite from proeutectoid ferrite and reduces the soluble carbon of ferrite [24], which results in a lower carbon content of ferrite (C_f) and higher C_m in DP steels. The HSi steel with carbide-free ferrite and fine, carbon-enriched austenite was therefore obtained. During phase transformation from austenite to martensite, the carbon-en-

riched austenite was transformed to higher-carbon martensite (0.32wt% C), which had a higher strength because the strength of martensite is very carbon dependent. This result shows that the carbon-enriched austenite transformed into glossy, angular martensite while the low carbon content austenite transformed into the veined martensite with irregular phase boundaries observed in SEM.

3.2. Microstructures evolution during hole expansion

To study the deformation mechanisms of different steels during the hole-expansion tests, microstructures near the deformed center hole along the circumferential direction (Fig. 4) and radial direction (Fig. 5) were observed. Although the observed regions had endured a bending force along the radial direction, hole-expansion deformation near the center hole was mainly influenced by the tension in the tangential direction, which is similar to the tensile test [13].

For the HSi steel, the dispersely distributed, high carbon content martensite islands were hardly deformed while ferrite grains were stretched plastically. This is attributed to the incompatibility of plastic deformation located between the ferrite and martensite phases. The plastic deformation of ferrite is constrained at the F–M phase boundaries, which finally leads to decohesion of the F–M phase boundaries or fracture of the brittle martensite islands [7]. Previous work [7,25–27] has described the void nucleation mechanism during tensile tests. In this work, decohesion at the F–M phase boundaries and separation of fractured martensite particles were observed in hole-expansion tests. Fig. 4 shows that voids formed at the F–M phase boundaries or at the sites where martensite particles fractured. This is similar to the results of Avramovic-Cingara *et al.* [28] during uniaxial tensile testing. Fig. 4(b) reveals that LSi experiences a larger plastic deformation than HSi. During *in-situ* tensile testing, Ghadbeigi *et al.* [14] found that the martensite phase experienced large plastic deformation of 110% for an applied strain of 42%, while the value of the ferrite phase was 130%. This confirms that martensite can also endure large deformation, similar to ferrite. Fig. 5 reveals the number and appearance of sites of void nucleation along the radial direction near the edge of the center hole. More microvoids were generated in the HSi steel than in the LSi steel.

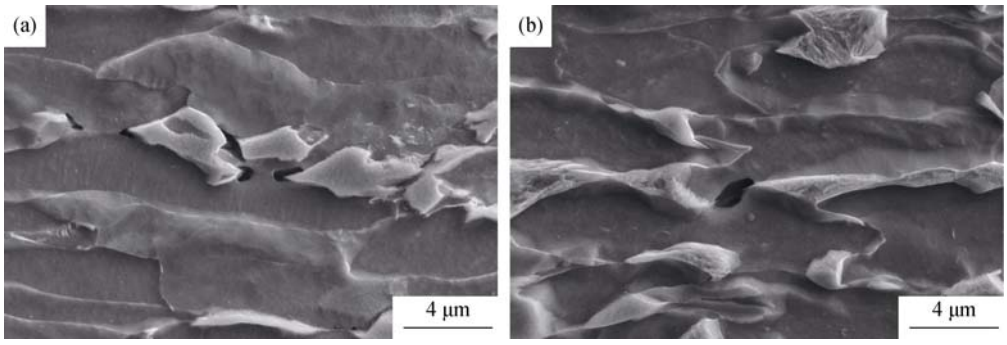

Fig. 4. Microstructures in the circumferential direction near the center hole: (a) HSi steel and (b) LSi steel.

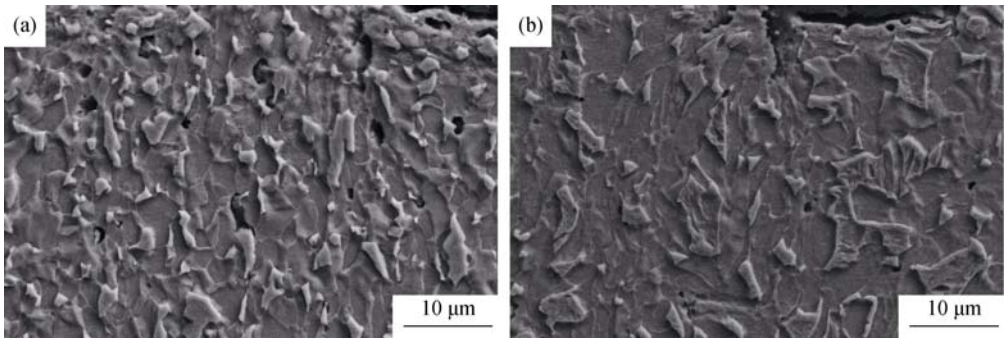

Fig. 5. Microstructures in the radial direction near the center hole: (a) HSi steel and (b) LSi steel.

The following two reasons probably explain the phenomena observed in Fig. 4 and Fig. 5: (1) martensite with low carbon content reduces the incompatibility of the two phases, and (2) martensite with a large curvature radius (due to the large size of martensite) weakens the effect of stress concentration on the angular sites of martensite.

Typical TEM micrographs after hole-expansion are shown in Fig. 6. TEM observations in the ferrite regions (Figs. 6(a) and 6(c)) reveal that after being stretched along the circumference direction and being bent in the perpen-

dicular-to-circumference direction, dislocations and dislocation cells tangled in ferrite grains and F–M phase boundaries are seen. As the mobile dislocations pile up in the vicinity of the F–M phase boundaries (arrow in Fig. 6(c)), some high-density tangled dislocations evolve into cell structures. TEM observations in the martensite region (Figs. 6(b) and 6(d)) reveal that the martensite in the LSi steel possessed lath morphology, while some twin martensite was found in the HSi steel.

It can be concluded from the TEM micrographs that in the initial stage of hole-expansion, dislocations sweep through ferrite grains and pile up in F–M phase boundaries. After that, martensite islands are surrounded by tangled dislocations and are forced to deform. Microvoids appear when the stress concentration exceeds the ultimate strength of martensite or the interfacial strength.

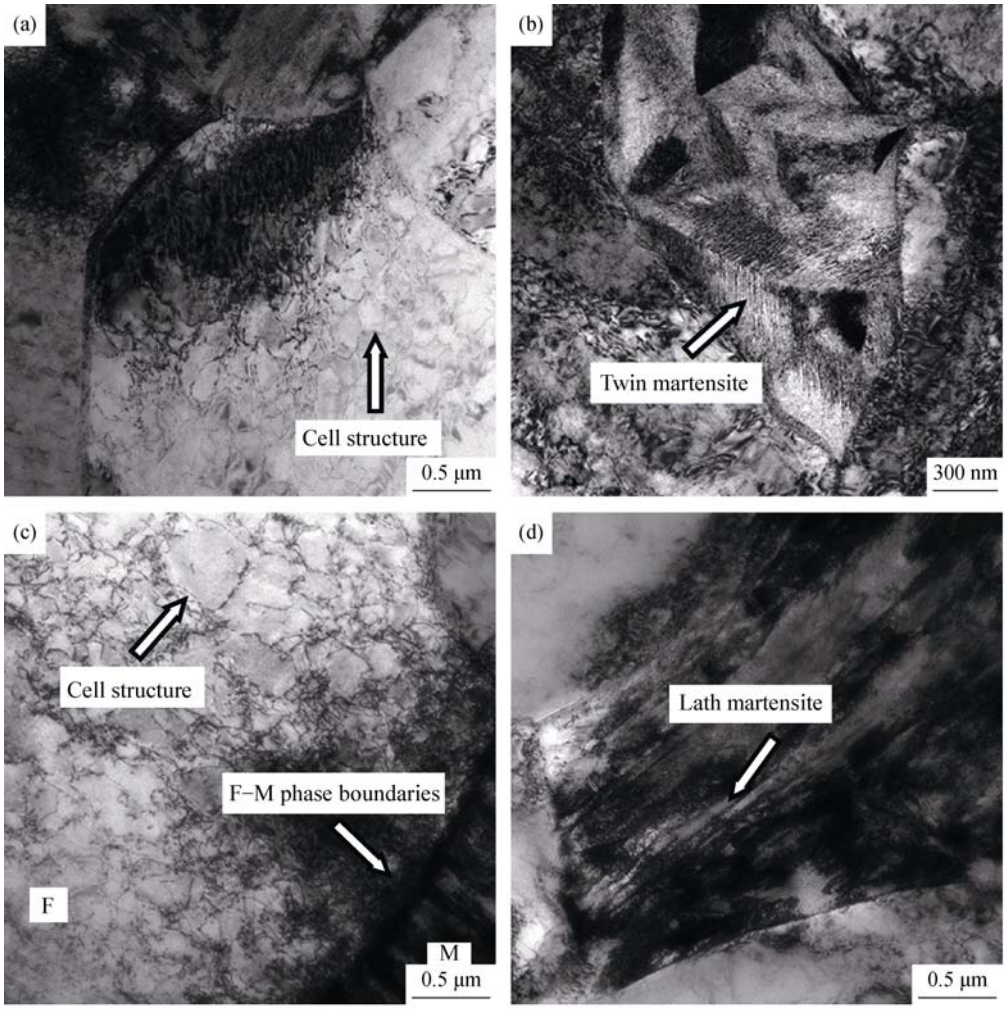

Fig. 6. TEM micrographs of test steels: (a, b) HSi steel; (c, d) LSi steel.

3.3. Mechanical properties

Fig. 7 shows the engineering stress–strain curves of experimental steels. For each steel, only one of the three tensile tests is shown, because the test data decentralities for each series are rather small. Both steels show the typical behavior of ferrite/martensite DP steels: high initial strain-hardening rate, the absence of a distinct yield point, and continuous yielding. With increasing silicon content, the ultimate tensile strength (UTS) and uniform elongation (UE) increase while the yield strength (YS) and total elongation (TE) decrease.

The strength of a dual-phase structure is dependent on the ferrite grain size and the martensite volume fraction [29]. A finer ferrite grain size, higher solution strength of silicon in ferrite grains, and higher strength of martensite lead to a higher UTS of HSi. Due to the effect of the dispersion strength of fine martensite islands, the UE of HSi reaches 18.2%. the YS of HSi is lower than that of LSi. This is attributed to the existence of abundant mobile dislocations.

The number of martensite islands in HSi is greater but the size is smaller, which increases the number of ferrite and martensite phase boundaries. When phases transform from austenite to martensite, with the action of volume expansion, plenty of mobile dislocations are generated near F–M phase boundaries. In the early stage of stretching, dislocations sweep past ferrite grains and tangle on F–M phase boundaries and decrease the YS. Although the addition of Si strengthens ferrite, which can increase YS, the appearance of numerous mobile dislocations has far more effect in decreasing the YS. In the process of stretching, stresses are transferred from work-hardened phases to unwork-hardened phases. As a result, many ferrite grains deform uniformly before necking. This is beneficial for increasing the UE and delaying the occurrence of necking.

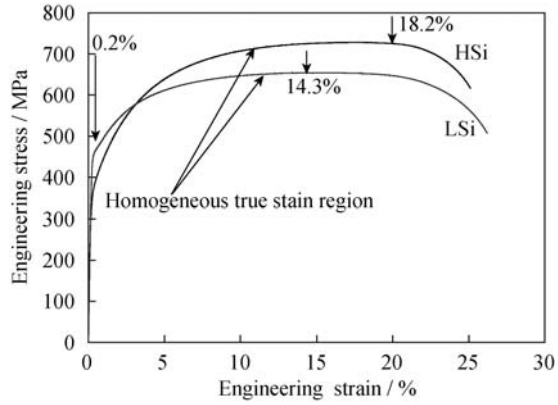

Fig. 7. Engineering stress–strain curves of the HSi and LSi steels.

The higher TE of LSi is due to its excellent ability for post-uniform deformation. Fig. 4 reveals that martensite in LSi experienced sharply plastic deformation. This demonstrated that martensite with low carbon content is easily deformed in coordination with ferrite in the post-uniform deformation stage.

3.4. Strain-hardening behavior

To analyze work-hardening characteristics of samples during tensile deformation, the Hollomon, Crussard–Jaoul, and modified Crussard–Jaoul analyses were used.

(1) Hollomon analysis.

Earlier analyses of the work-hardening behavior of many metals and alloys can be described by the Hollomon relation [30] as follows:

$$\sigma_t = k\varepsilon_t^n \tag{3}$$

where k is the strain-hardening coefficient, n is the work-hardening exponent, σ_t is the true stress, and ε_t is the true strain. The results of the Hollomon analysis are shown in Fig. 8. Earlier studies [31–33] indicated that DP steels show two-stage hardening followed by two work-hardening indices. In this study, however, the Hollomon's plots show that both steels followed a linear variation of ln σ_t versus ln ε_t with a nearly constant n value (Table 2). The LSi steel has a smaller n value than the His steel. In the opinion of Kumar *et al.* [5], the n value decreases with increasing martensite volume fraction. This may be attributed to localized ferrite plastic strain (LFPS). The LFPS is influenced by the extent of the plastic zone in ferrite, the average dislocation density, and the associated strain in ferrite. As the martensite volume fraction increases in DP steels, localized plastic strain increases and, consequently, the overall true uniform plastic strain decreases.

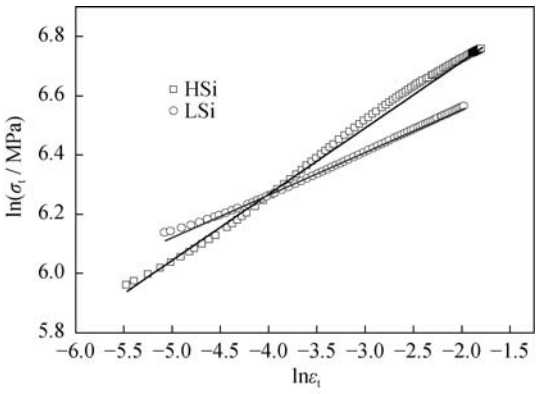

Fig. 8. Holloman's plots of ln(σ_t) versus lnε_t for the HSi and LSi steels.

Table 2. Summary of parameters related to the work-hardening behavior of HSi and LSi DP steels

Steel	Hollomon's analysis	D_{C-J} analysis					M_{C-J} analysis		
	Slope (n)	Slope ($n'-1$)			Transition strain / %		Slope ($1-n''$)		Transition train / %
		Stage-I	Stage-II	Stage- III	I to II	II to III	Stage-I	Stage-II	
HSi	0.22	–1.66	–0.36	–0.94	–5.55	–3.99	–2.04	–4.78	3.39
LSi	0.14	–3.64	0.08	–0.79	–5.61	–4.78	–4.25	–5.84	2.68

(2) Differential Crussard–Jaoul analysis.

The differential Crussard–Jaoul (D_{C-J}) analysis [34–35] of the tensile stress–strain curves has been used in many kinds of alloys and is based on the power Ludwik relation expressed as follows:

$$\sigma_t = \sigma_0 + k'\varepsilon_t^{n'} \tag{4}$$

where σ_t is the true stress, ε_t is the true strain, n' is the work-hardening exponent, and σ_0 and k' are material constants. The logarithmic form of Eq. (4) after differentiation with respect to ε_t is as follows:

$$\ln\frac{d\sigma_t}{d\varepsilon_t} = \ln(k'n') + (n'-1)\ln\varepsilon_t \quad (5)$$

The D_{C-J} analyses of tensile data for both steels have been carried out using Eq. (5), as shown in Fig. 9. These plots indicate that the flow stress behavior of both DP steels can be described using a three-stage work-hardening behavior. The three stages observed may be due to different work-hardening mechanisms associated with the finer distribution of constituent phases [18].

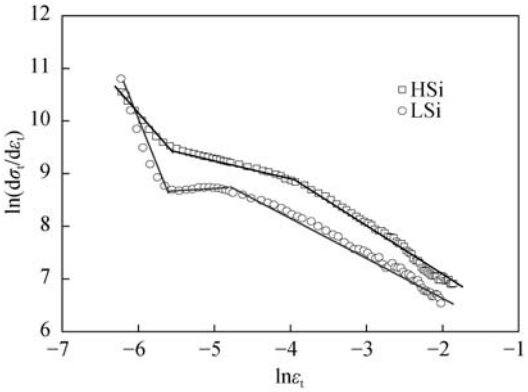

Fig. 9. Differential Crussard–Jaoul plots of $\ln(d\sigma_t/d\varepsilon_t)$ vs. $\ln\varepsilon_t$ for the HSi and LSi steels.

Several previous investigators [18,31,33,36] have been able to reveal the three stages of work hardening in DP steels using D_{C-J} analyses, which can be attributed to the following deformation mechanisms.

Stage I: Homogeneous deformation of the ferrite matrix assisted by the glide of mobile dislocations present near the martensite regions.

Stage II: Diminished work hardening due to the deformation of constrained ferrite with the possible transformation of retained austenite to martensite.

Stage III: Ferrite deformation with attendant cross-slip and dynamic recovery together with martensite deformation.

The values of $n'-1$ at these separate stages are given in Table 2. The absolute value of $n'-1$ for HSi is smaller than that for LSi in stage I, while in the transition region, stage II, the result is just the opposite. In stage III, the two values of $n'-1$ are similar. The negative value of $n'-1$ in both stage I and stage III have been reported in several investigations [33,35,37] of DP steels. A high value of $n'-1$ in stage I is due to homogeneous deformation of ferrite. The rate of work hardening is high in this stage because undissolved carbide particles impede the glide of dislocations in the ferrite phase [32]. Das and Chattopadhyay [33] attributed this to the presence of a high internal stress field caused by a high density of lattice defects and/or microstructure heterogeneity. The onset of stage III is associated with the onset of cross-slip and dynamic recovery effects in ferrite, e.g., rearrangement of dislocation structures and annihilation of dislocations [37]. The presence of stage II may be due to dynamic changes of internal stresses during plastic deformation [32].

(3) Modified Crussard–Jaoul analysis.

The modified Crussard–Jaoul analysis (M_{C-J}) has been suggested as suitable for analyzing the hardening behavior of DP steels [38]. It is based on the Swift equation:

$$\varepsilon_t = \varepsilon_0 + k''\sigma_t^{n''} \quad (6)$$

where σ_t is the true stress; ε_t is the true strain; ε_0 is the initial true strain; n'' is the work-hardening exponent, and k'' is the material constant. Differentiating Eq. (6) with respect to ε_t and expressing in the logarithmic form, we get the following equation:

$$\ln\frac{d\sigma_t}{d\varepsilon_t} = (1-n'')\ln\sigma_t - \ln(k''n'') \quad (7)$$

In this work, the M_{C-J} analysis reveals two stages of strain hardening for both steels during the uniform tension process, as shown in Fig. 10.

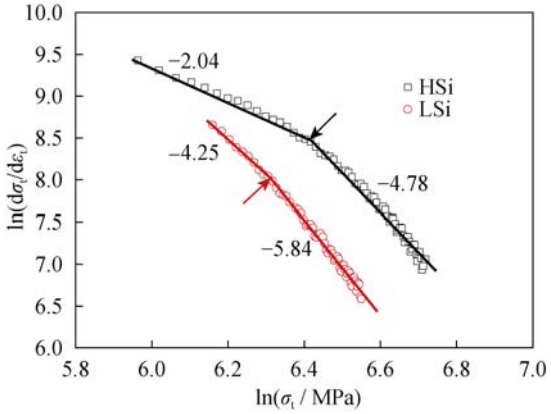

Fig. 10. Plots of $\ln(d\sigma_t/d\varepsilon_t)$ vs. $\ln\sigma_t$ for the modified Crussard–Jaoul analysis of the HSi and LSi steels. Slopes of different stages are shown.

Several earlier observations [4,33,38–41] revealed two distinct stages of work hardening in $\ln(d\sigma_t/d\varepsilon_t)$ vs. $\ln\sigma_t$ curves of DP steels by the M_{C-J} technique. The two stages of work hardening observed in F–M DP steels are attributed to the following deformation mechanisms.

Stage I: Plastic deformation of the soft ferrite matrix alone assisted by mobile dislocations present near the mart-

ensite regions, while the martensite phase is in elasticity.

Stage II: Uniform deformation of hard martensite and already work-hardened ferrite.

It is apparent that the values of $1 - n''$ for both stage I and stage II deformations are comparable (Table 2). The transition value, ε_t, which is considered to be the strain where both phases begin to deform plastically, from stage I to stage II varies significantly with the variation of microstructure characteristics. The slope in the first stage is larger. This is attributed to the fact that ferrite grains are plastically restrained by carbide precipitates in the ferrite grains and surrounding martensite during plastic deformation [41]. For the LSi steel, the first stage will continue to a smaller strain, and for that martensite will begin to deform plastically earlier [39].

The results of the D_{C-J} and M_{C-J} analyses (Fig. 9 and Fig. 10) are in accordance with those of Das and Chattopadhyay [33]. The M_{C-J} analysis sensitively captures the transition of work hardening from ferrite-dominated to martensite-dominated regimes while the D_{C-J} analysis reveals the transitional stage of constrained plasticity of ferrite induced by martensite particles.

3.5. Hole-expansion tests

Fig. 11 shows specimen shapes and Fig. 12 shows the load-displacement curves of each steel during hole-expansion tests. In the first stage (before the knee, as arrows show), the load value increases when the punch touches the work piece. This is followed by a linear evolution linked to the elastic deformation [42]. The deflection of the edge is the principal deformation (after the knee). At this stage, the punch load value increases non-linearly with punch travel [42]. The hole circumferentially expands by bending and stretching until a crack appears in the hole edge and the load value begins to decrease. Pieces of deformed lips were machined by wire-electrode cutting parallel to the radial direction planes from the hole-expanded samples, as shown in Fig. 13(a). An area ratio method, which has been used by Hyun *et al.* [8], is applied in this paper to compare the degrees of deformation of both steels. The ratio of hatched area A to base area B is defined as schematically shown in Fig. 13(b). The area A, area B, lip thickness, and lip height of both steels were estimated from Fig. 13(a).

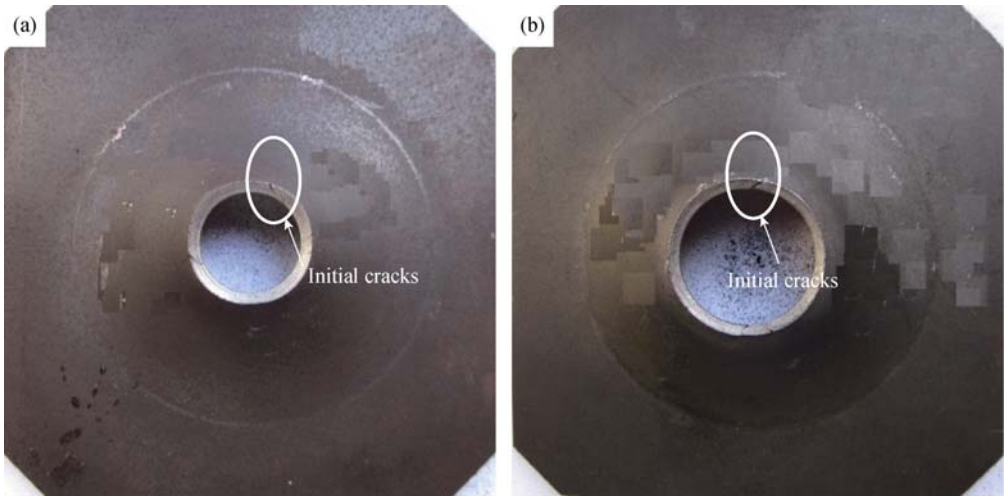

Fig. 11. Specimen shapes after hole-expanding tests: (a) His steel; (b) LSi steel .

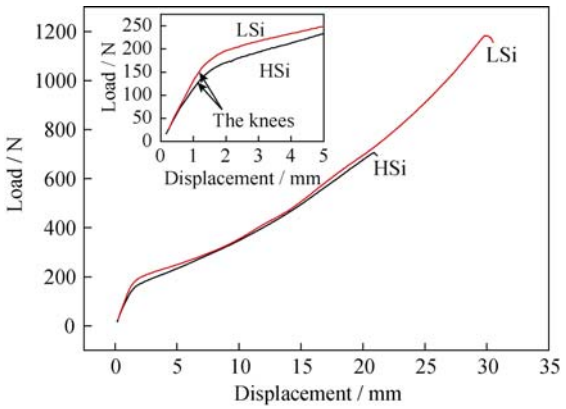

Fig. 12. Load−displacement curves of the HSi and LSi steels.

The lip thickness, lip height, areas A and B, and the ratio value of A/B are shown in Table 3. This shows that area A, area B, and area ratio (A/B) are related to λ. The sample with a high value of λ has high values of A and B. Meanwhile, the high-λ sample has a smaller lip thickness and a larger lip height. This means that LSi experiences a larger deformation along the radial direction and reduction in the thickness direction. Curves in Fig. 12 reveal that the HSi steel has a poor toughness because its load value is smaller than that of LSi.

Hasegawa *et al.* [43] have confirmed that the difference in strength of ferrite and martensite is an effective factor in

improving the stretch-flangeability of DP steels. Due to a smaller difference in hardness and strength between ferrite and martensite for LSi, LSi has a better deformation ability in three dimensions. This is attributed to a better plastic incompatibility of ferrite and martensite, which makes the strain distribution in the two phases more uniform during the high strain stage. The production and decohesion of microvoids are therefore delayed.

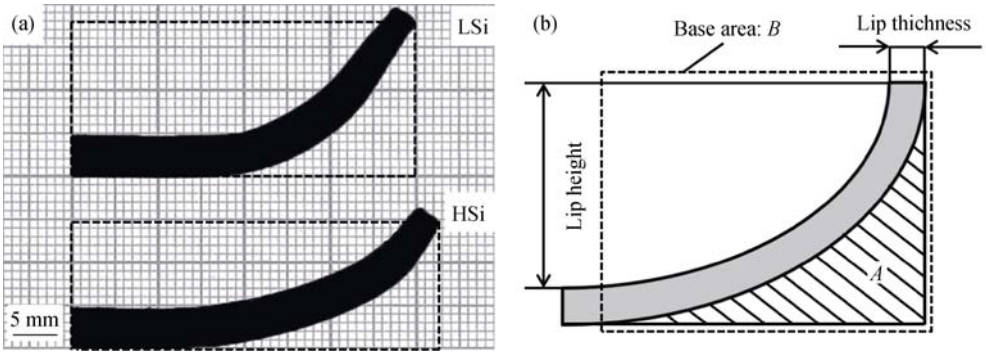

Fig. 13. Shape and size of deformed lips the HSi and LSi steels.

Table 3. Parameters of hole-expansion test for HSi and LSi DP steels

Steel	A / mm^2	B / mm^2	A/B	Lip thickness / mm	Lip height / mm	λ / %
HSi	118	466	0.253	2.62	14.4	76
LSi	129	535	0.241	2.33	17.4	130

In the high strain stage, more dislocations tangle in F–M boundaries and surround martensite in HSi. This leads to strong stress concentration and the appearance of microvoids occurs easily in the fragile F–M phase boundaries. When microvoids extend and pass through the fragile martensite or F–M phase boundaries, cracks will occur. Macrocracks will therefore appear at an earlier stage with a low post-uniform deformation.

4. Conclusions

Two kinds of DP steels with different silicon contents were produced by the same thermal treatment process. Their mechanical properties were studied based on tensile and hole-expansion test data and microstructure observations. The main conclusions are as follows.

(1) The grain sizes of ferrite and martensite are significantly refined by the addition of Si up to 1.08wt%. Si promotes the phase transformation of proeutectoid ferrite and leads to low martensite volume fraction and high carbon content in martensite.

(2) The addition of 1.08wt% Si leads to the increase of UTS and UE, but the decrease of YS, yield ratio, and λ-value. The Hollomon analysis indicates that the increase of martensite volume fraction leads to a decrease of the strain-hardening exponent (n value), which finally leads to a decrease of uniform elongation. The D_{C-J} analysis reveals that the transitional stage of the constrained plasticity of ferrite is induced by martensite particles while the M_{C-J} analysis sensitively captures the transition of work hardening from ferrite-dominated to martensite-dominated regimes.

(3) In hole-expansion tests, microvoids are generated at the F–M phase boundaries or the sites where martensite fractures. In the high strain stage, LSi has a better ability to coordinate deformation between ferrite and martensite phases than HSi. The good stretch-flangeability of LSi is attributed to crack suppression during propagating in the post-uniform deformation stage.

Acknowledgements

This work was financially supported by the Fundamental Research Funds for the Central Universities of China (No. FRF-TP-12-046A) and the Beijing Higher Education Young Elite Teacher Project (No. YETP0355).

References

[1] M. Calcagnotto, D. Ponge, and D. Raabe, Effect of grain refinement to 1μm on strength and toughness of dual-phase steels, *Mater. Sci. Eng. A*, 527(2010), p. 7832.

[2] H.F. Dong, J. Li, Y. Zhang, J. Park, and Q.X. Yang, Numerical simulation on the microstress and microstrain of low Si-Mn-Nb dual-phase steel, *Int. J. Miner. Metall. Mater.*, 17(2010), No. 2, p. 173.

[3] J. Lee, S.J. Lee, and B.C. De Cooman, Effect of micro-alloying elements on the stretch-flangeability of dual phase steel, *Mater. Sci. Eng. A*, 536(2012), p. 231.

[4] Y. Tomita, Effect of morphology of second-phase martensite on tensile properties of Fe–0.1C dual phase steels, *J. Mater. Sci.*, 25(1990), p. 5179.

[5] A. Kumar, S.B. Singh, and K.K. Ray, Influence of bainite/martensite-content on the tensile properties of low carbon dual-phase steels, *Mater. Sci. Eng. A*, 474(2008), p. 270.

[6] Z.G. Wang, A.M. Zhao, Z.Z. Zhao, J.Y. Ye, D. Tang, and G.S. Zhu, Microstructures and mechanical properties of C-Mn-Cr-Nb and C-Mn-Si-Nb ultra-high strength dual-phase steels, *Int. J. Miner. Metall. Mater.*, 19(2012), No. 10, p. 915.

[7] D.L. Steinbrunner, D. Matlock, and G. Krauss, Void formation during tensile testing of dual phase steels, *Metall. Trans. A*, 19(1988), p. 579.

[8] D.I. Hyun, S.M. Oak, S.S. Kang, and Y.H. Moon, Estimation of hole flangeability for high strength steel plates, *J. Mater. Process. Technol.*, 130-131(2002), p. 9.

[9] J.H. Kim, M.G. Lee, D. Kim, D.K. Matlock, and R.H. Wagoner, Hole-expansion formability of dual-phase steels using representative volume element approach with boundary-smoothing technique, *Mater. Sci. Eng. A*, 527(2010), p. 7353.

[10] K.I. Mori, Y. Abe, and Y. Suzui, Improvement of stretch flangeability of ultra high strength steel sheet by smoothing of sheared edge, *J. Mater. Process. Technol.*, 210(2010), p. 653.

[11] K.I. Sugimoto, T. Muramatsu, S.I. Hashimoto, and Y. Mukai, Formability of Nb bearing ultra high-strength TRIP-aided sheet steels, *J. Mater. Process. Technol.*, 177(2006), p. 390.

[12] A. Nagasaka, K. Sugimoto, and M. Kobayashi, Effect of second phase morphology on warm stretch-flangeability in high strength TRIP-aided dual-phase steel sheets, [in] *ASM International* (*USA*), New York, 1996, p. 557.

[13] Y. Yamada and M. Koide, Analysis of the bore-expanding test by the incremental theory of plasticity, *Int. J. Mech. Sci.*, 10(1968), p. 1.

[14] H. Ghadbeigi, C. Pinna, S. Celotto, and J.R. Yates, Local plastic strain evolution in a high strength dual-phase steel, *Mater. Sci. Eng. A*, 527(2010), p. 5026.

[15] M. Sarwar and R. Priestner, Influence of ferrite-martensite microstructural morphology on tensile properties of dual-phase steel, *J. Mater. Sci.*, 31(1996), p. 2091.

[16] S. Kim and S. Lee, Effects of martensite morphology and volume fraction on quasi-static and dynamic deformation behavior of dual-phase steels, *Metall. Mater. Trans. A*, 31(2000), p. 1753.

[17] K.J. Kim, S. Lee, and C. Lee, Effects of martensite morphology on dynamic torsional behavior in dual phase steels, *Scripta Mater.*, 38(1997), No. 1, p. 27.

[18] A. Bag, K.K. Ray, and E.S. Dwarakadasa, Influence of martensite content and morphology on the toughness and fatigue behavior of high-martensite dual-phase steels, *Metall. Mater. Trans. A*, 32(2001), p. 2207.

[19] E. Ahmad, T. Manzoor, M.M.A. Ziai, and N. Hussain, Effect of martensite morphology on tensile deformation of dual-phase steel, *J. Mater. Eng. Perform.*, 21(2012), No. 3, p. 382.

[20] M. Sudo, S. Hashimoto, and S. Kambe, Niobium bearing ferrite-bainite high strength hot-rolled sheet steel with improved formability, *Trans. Iron Steel Inst. Jpn.*, 23(1983), No. 4, p. 303.

[21] M.R. Akbarpour and A. Ekrami, Effect of ferrite volume fraction on work hardening behavior of high bainite dual phase (DP) steels, *Mater. Sci. Eng. A*, 477(2008), p. 306.

[22] M.H. Cai, H. Ding, J.S. Zhang, and L. Li, Effect of silicon and prior deformation of austenite on isothermal transformation in low carbon steels, *Acta Metall. Sin.*, 22(2009), No. 2, p. 100.

[23] M.H. Cai, H. Ding, Y.K. Lee, Z.Y. Tang, and J.S. Zhang, Effects of Si on microstructural evolution and mechanical properties of hot-rolled ferrite and bainite dual-phase steels, *ISIJ Int.*, 51(2011), No. 3, p. 476.

[24] G. Thomas and J.Y. Koop, Structure and properties of dual phase steel, [in] *The Metallurgical Society of AIME*, New York, 1979.

[25] A.H. Nakagawa and G. Thomas, Microstructure-mechanical property relationships of dual-phase steel wire, *Metall. Trans. A*, 16(1985), p. 831.

[26] D.A. Korzekwa, R.D. Lawson, D.K. Matlock, and G. Krauss, A consideration of models describing the strength and ductility of dual-phase steels, *Scripta Metall.*, 14(1980), p. 1023.

[27] G. Avramovic-Cingara, Y. Ososkov, M.K. Jain, and D.S. Wilkinson, Effect of martensite distribution on damage behaviour in DP600 dual phase steels, *Mater. Sci. Eng. A*, 516(2009), p. 7.

[28] G. Avramovic-Cingara, Ch.A.R. Saleh, M.K. Jain, and D.S. Wilkinson, Void nucleation and growth in dual-phase steel 600 during uniaxial tensile testing, *Metall. Mater. Trans. A*, 40(2009), p. 3117.

[29] R.G. Davies, Influence of martensite composition and content on the properties of dual phase steels, *Metall. Trans. A*, 9(1978), p. 671.

[30] J.H. Hollomon, Tensile deformation, [in] *The Metallurgical Society of AIME*, New York, 1945, p. 162.

[31] T.S. Byun and I.S. Kim, Tensile properties and inhomogeneous deformation of ferrite-martensite dual-phase steels, *J. Mater. Sci.*, 28(1993), p. 2923.

[32] A. Bag, K.K. Ray, and E.S. Dwarakadasa, Influence of martensite content and morphology on tensile and impact properties of high-martensite dual-phase steels, *Metall. Mater. Trans. A*, 30(1999), p. 1193.

[33] D. Das and P.P. Chattopadhyay, Influence of martensite morphology on the work-hardening behavior of high strength ferrite-martensite dual-phase steel, *J. Mater. Sci.*, 44(2009), p. 2957.

[34] P.B. Jaoul, Etude de la forme des courbes de deformation plastique, *J. Mech. Phys. Solids*, 5(1957), p. 95.

[35] S.N. Monteiro and R.E. Reed-Hill, On the double-*n* behavior

of iron, *Metall. Trans.*, 2(1971), No. 10, p. 2947.

[36] F.H. Samuel, D. Daniel, and O. Sudre, Further investigations on the microstructure and mechanical behaviour of granular bainite in a high strength, low alloy steel: comparison of ferrite-pearlite and ferrite-martensite microstructures, *Mater. Sci. Eng.*, 92(1987), p. 43.

[37] S. Sankaran, S. Sangal, and K.A. Padmanabhan, Microstructural evolution and tensile behaviour of medium carbon microalloyed steel processed through two thermomechanical routes, *Mater. Sci. Technol.*, 21(2005), No. 10, p. 1152.

[38] Y. Tomita and K. Okabayashi, Mechanical properties of 0.40 pct C-Ni-Cr-Mo high strength steel having a mixed structure of martensite and bainite, *Metall. Trans. A*, 16(1985), p. 73.

[39] Z.H. Jiang, Z.Z. Guan, and J.S. Lian, The relationship between ductility and material parameters for dual-phase steel, *J. Mater. Sci.*, 28(1993), p. 1814.

[40] Y.I. Son, Y.K. Lee, K.T. Park, C.S. Lee, and D.H. Shin, Ultrafine grained ferrite–martensite dual phase steels fabricated via equal channel angular pressing: microstructure and tensile properties, *Acta Mater.*, 53(2005), p. 3125.

[41] Y. Tomita and K. Okabayashi, Tensile stress-strain analysis of cold worked metals and steels and dual-phase steels, *Metall. Trans. A*, 16(1985), p. 865.

[42] A. Kacem, A. Krichen, and P.Y. Manach, Occurrence and effect of ironing in the hole-flanging process, *J. Mater. Process. Technol.*, 211(2011), p. 1606.

[43] K. Hasegawa, K. Kawamura, T. Urabe, and Y. Hosoya, Effects of microstructure on stretch-flange-formability of 980 MPa grade cold-rolled ultra high strength steel sheets, *ISIJ Int*., 44(2004), No. 3, p. 603.